ADVANCED MATERIALS INTERFACES
www.advmatinterfaces.de

Hexagonal Boron Nitride Nanosheets Protect Exfoliated Black Phosphorus Layers from Ambient Oxidation

Cora Bartus Pravda, Tímea Hegedűs, Eliezer Fernando Oliveira, Dániel Berkesi, Ákos Szamosvölgyi, Zoltán Kónya, Róbert Vajtai, and Ákos Kukovecz**

Black phosphorus-based 2D materials have yet to demonstrate their full application potential because of the well-known sensitivity of phosphorene to spontaneous oxidation under ambient conditions. It is hypothesized that this unfavorable process can be prevented by drop-casting hexagonal boron nitride (h-BN) nanosheets on phosphorene. Here, both materials are prepared by sonication-assisted liquid-phase exfoliation of bulk materials and characterized by transmission electron microscopy and Raman spectroscopy. Raman spectroscopy is also utilized for the real-time monitoring of phosphorene oxidation by calculating the A_{1g}/A_{2g} intensity ratio. This value drops below 0.5 (corresponding to complete oxidation) within 100 min for pristine phosphorene layers in the air. However, it remains constant above 0.6 (indicating no oxidation) when phosphorene covered by h-BN sheets is left in the air. Moreover, deploying h-BN sheets at midterm during the ambient oxidation reaction is able to halt the process and maintain a steady $0.5 < A_{1g}/A_{2g} < 0.6$ Raman intensity ratio. The experimental results are successfully interpreted within the developed theoretical framework by the charge distribution of h-BN, which keeps O_2 molecules from interacting with its surface, and the fact that the first O_2 molecules in contact react with the edges of h-BN, thus creating a barrier for subsequently arriving O_2 molecules.

1. Introduction

Two-dimensional materials like black phosphorus (BP), hexagonal boron nitride (h-BN), graphene, molybdenum disulfide, transition metal dichalcogenides, etc. are in the focus of scientific attention today because of their exceptional properties.[1,2] The individual phosphorene layers in BP are held together by van der Waals forces.[3] Every P atom forms sp^3 hybridized covalent bonds with the neighboring P atoms in phosphorene, the layers are therefore nonplanar as a puckered hexagonal structure.[4,5] BP is a direct bandgap p-type semiconductor[6] and its bandgap ranges from 0.3 eV for bulk BP to 2 eV in the case of phosphorene.[7] The bandgap is tunable and depends on a variety of characteristics of the material, including the number of layers.[8] BP can absorb light in a wide wavelength[4] and be applied in optoelectronics in the infrared range.[9] It has been proposed for application in humidity sensors,[10,11] electrochemical sensors,[12] and gas sensors.[13,14] Medical-biomedical applications, electrochemical immune sensors, optoelectronic and photonic devices are also considered.[12,15–18]

Layered materials research in the past few years was concerned with tailoring their properties in terms of increasing their stability under ambient conditions.[19–21] Compared to other 2D materials, phosphorene oxidizes more rapidly, since it has both a free electron pair in each sp^3 hybridized phosphorus atom and a high surface to volume ratio.[22] The instability of phosphorene flakes in ambient conditions is a major drawback hindering their practical applications[16,23,24] because only non-oxidized monolayers exhibit the desired properties in near-IR applications.[25] Pristine phosphorene flakes oxidize in the air within a couple of hours and this is accompanied by a bandgap increase.[26] A way to overcome this is passivation by depositing inert hetero-layers on the sensitive layer. The resulting structures are held together by noncovalent interactions and are commonly referred to in the literature as van der Waals structures.[27–30]

Nanosheets of h-BN, called white graphene,[2] are the most stable crystalline form of BN featuring a planar hexagonal, honeycomb-like structure[31] similar to graphene. The hexagonal

C. Bartus Pravda, T. Hegedűs, D. Berkesi, Á. Szamosvölgyi, Z. Kónya, Á. Kukovecz
Interdisciplinary Excellence Centre
Department of Applied and Environmental Chemistry
University of Szeged
Rerrich Béla tér 1, Szeged H-6720, Hungary
E-mail: kakos@chem.u-szeged.hu

E. F. Oliveira
São Paulo State Department of Education
São Paulo, Brazil

Z. Kónya
MTA-SZTE
Reaction Kinetics and Surface Chemistry Research Group
University of Szeged
Rerrich Béla tér 1, Szeged H-6720, Hungary

R. Vajtai
Department of Materials Science and NanoEngineering
Rice University
6100 Main Street, Houston, Texas 77005, USA
E-mail: robert.vajtai@rice.edu

The ORCID identification number(s) for the author(s) of this article can be found under https://doi.org/10.1002/admi.202200857.

DOI: 10.1002/admi.202200857

 © 2022 Wiley-VCH GmbH

21967350, 2022, 24, Downloaded from https://onlinelibrary.wiley.com/doi/10.1002/admi.202200857 by University Of Szeged, Wiley Online Library on [03/07/2023]. See the Terms and Conditions (https://onlinelibrary.wiley.com/terms-and-conditions) on Wiley Online Library for rules of use; OA articles are governed by the applicable Creative Commons License

lattice consists of an equal number of alternating B and N atoms in sp^2 configuration. The bond is covalent with a partially ionic character that leads to a so-called "lip–lip" interaction between the layers.[32] Exfoliated h-BN layers exhibit an optical absorption peak at around 200 nm that stands for an ≈6 eV bandgap.[33,34] Due to the high in-plane thermal conductivity of h-BN, it can be used in high-temperature applications.[35] Moreover, it has also been reported for covering and passivating other materials that oxidize easily.[36] Hetero-layers of graphene and h-BN have already been reported in several publications where the goal was to open the bandgap of graphene and tune its value.[37–39]

Combinations of h-BN with phosphorene are also possible. A number of papers have conducted theoretical research on encapsulating phosphorene within h-BN to reveal how this protects it from oxidation under ambient conditions while keeping its beneficial properties.[19,25,40] Some researchers used h-BN to protect phosphorene and investigated its possible applications as field-effect transistors[41] and compared the charge transfer characteristics with the pristine nanosheets.[24,42] Mechanically exfoliated phosphorene was transferred onto h-BN grown by chemical vapor deposition in order to make them air-stable and the protection efficiency was confirmed by AFM measurements, they have concluded that the heterostructure does not show degradation in the observed time period.[43] The h-BN affects the vibrational properties of the encapsulated phosphorene.[44] The electronic structure of the heterostructure remains intact, however, the A_{1g} high-frequency optical mode of the phosphorene suffers a redshift of up to 10 cm^{-1} when in contact with h-BN layers.[44] The effect of vacancies and other impurities on the h-BN heterostructures with BP has been recently investigated with simulations, it has been concluded that these defects may change the electronic structures.[45] Despite the aforementioned efforts, no experimental evidence based on simple and scalable exfoliated materials has been published about the protective effect of h-BN on few-layered BP until now.

We hypothesize that insulating monolayers of h-BN can solve the oxidation sensitivity issues of BP. In the present study, the exfoliation of h-BN and BP was conducted separately in the liquid phase, because this method offers more control over the size of the flakes than mechanical exfoliation.[46] The exfoliated nanomaterials were characterized by transmission electron microscopy (TEM) and Raman spectroscopy. Then, the oxidation of BP layers under ambient conditions and the effect of h-BN nanosheets on their stability under ambient conditions was followed by real-time Raman spectroscopy, which is an effective technique for monitoring both the layer thickness of BP[3] and its oxidation state.[47–49] Raman spectroscopy was previously applied for investigating the changes in the Raman modes of BP when encapsulated with h-BN,[50] however, this is the first time that time-dependent Raman measurements were used to determine the oxidation process of phosphorene and the fabricated heterostructure. Theoretical simulations were performed to understand in which way the h-BN can prevent BP oxidation and how the oxygen molecule approaches the materials. These results provide a new method to follow the oxidation of phosphorene under ambient conditions and to preserve a partially oxidized state of phosphorene.

2. Results and Discussion

Our research approach is summarized in **Figure 1**. The top path illustrates the well-known spontaneous degradation of BP that serves as a benchmark. The dispersion of exfoliated BP flakes is dried on a Si wafer and allowed to oxidize in ambient air (Figure 1a). In the middle path (Figure 1b), the drop-cased BP sample is allowed to oxidize for a while, then it is covered by exfoliated h-BN sheets and its oxidation state

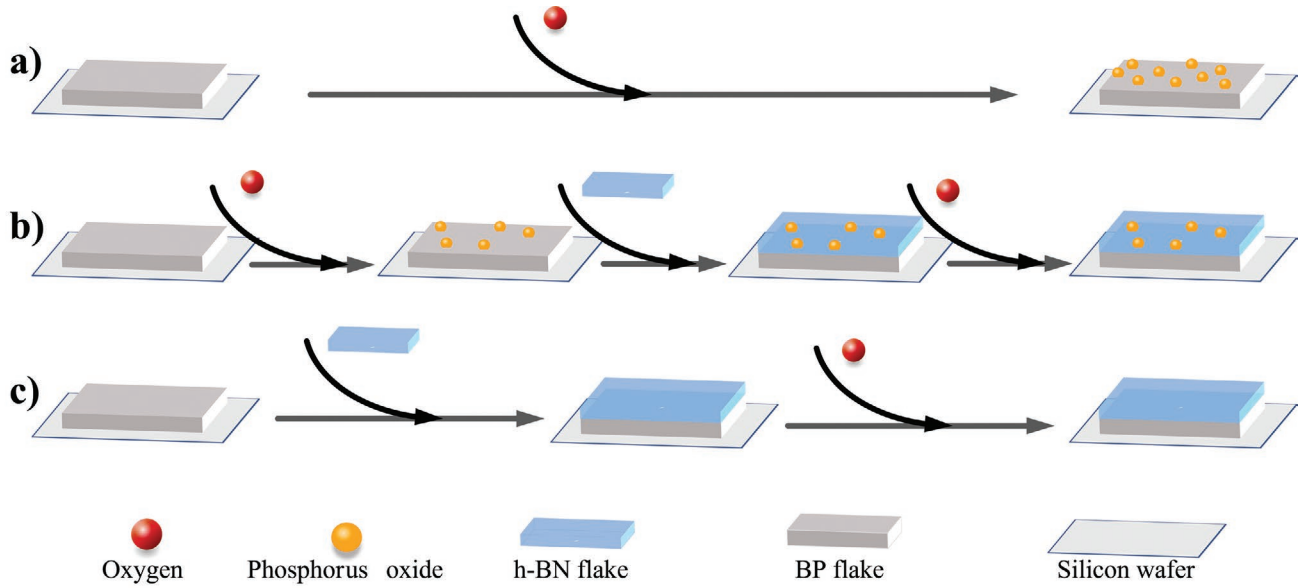

Figure 1. Block diagram of the measurement steps, a) full oxidation of BP b) protection of the partially oxidized BP sample by addition of h-BN c) protection of the BP from oxidation. The term "Phosphorus oxide" denotes all phosphorene oxidation species.

© 2022 Wiley-VCH GmbH

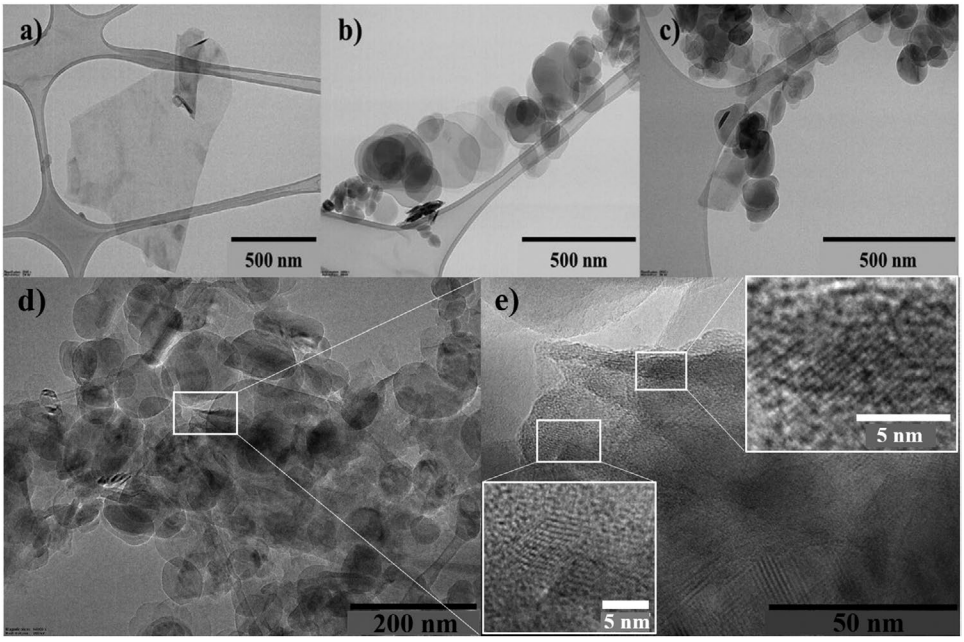

Figure 2. Transmission electron microscopy (TEM) image of a) exfoliated BP, b) exfoliated h-BN, and c) BP sheet well-covered with h-BN sheets. Part (d) depicts an almost completely covered BP flake with just a small phosphorene corner visible under the h-BN layers, while part e) presents this corner in more detail. Left and right insets in part (e) show BP and h-BN atomic layers, respectively.

is monitored further. In this case, BP maintains the oxidation state it was when the h-BN coating was applied. The bottom path (Figure 1c) depicts the route where the protective h-BN coating is applied directly after drop-casting the BP flakes, and consequently, the oxidation of the phosphorene layer is fully prevented.

The BP and h-BN flakes exfoliated in acetone were characterized by TEM. The images in **Figure 2** evidence that the exfoliation was successful for both materials. In Figure 2a an angular mono-layered BP flake can be seen, while Figure 2b shows exfoliated h-BN flakes that are smaller in diameter and have a round shape. The TEM image of a BP sheet well-covered with

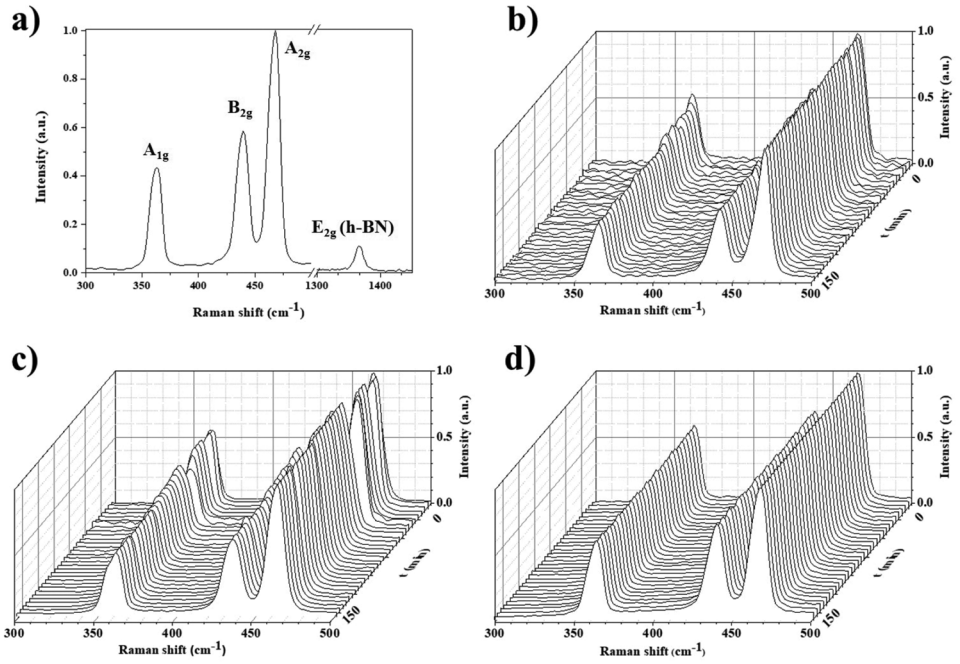

Figure 3. a) Raman spectrum of exfoliated black phosphorus and h-BN. Time series Raman spectra characteristic of the ambient oxidation process of b) unprotected BP, c) BP covered by h-BN after 50 min of oxidation, and d) BP covered by h-BN right from the start. All BP peaks are intensity normalized to the A_{2g} peak.

© 2022 Wiley-VCH GmbH

21967350, 2022, 24, Downloaded from https://onlinelibrary.wiley.com/doi/10.1002/admi.202200857 by University Of Szeged, Wiley Online Library on [03/07/2023]. See the Terms and Conditions (https://onlinelibrary.wiley.com/terms-and-conditions) on Wiley Online Library for rules of use; OA articles are governed by the applicable Creative Commons License

layers of h-BN is presented in Figure 2c. Almost complete BP coverage is depicted in Figure 2d. Figure 2e presents a zoomed-in section of Figure 2d where the very corner of the underlying BP flake is visible below the h-BN layers.

The Raman spectrum of pristine BP has three characteristic peaks, corresponding to the A_{1g}, B_{2g}, and A_{2g} modes appearing at 362.5, 439.5, and 467.8 cm^{-1}, respectively (**Figure 3**a).[50,10] The Raman modes of thinner mono- or bilayer BP flakes shift toward higher values compared to bulk BP therefore it is an effective indicator for differentiating the thinner BP flakes.[3,51,52] With the decrease of BP layer thickness the A_{1g}, B_{2g}, and A_{2g} Raman modes show different peak shifting rates, 0.15, 0.11, and 0.11cm^{-1} nm^{-1}, respectively.[53] Observing the values of the characteristic Raman shifts in Figure 3a it can be concluded that our sample contained phosphorene. The oxidation state of BP correlates with the intensity ratio of the A_{1g} and A_{2g} Raman peaks.[54–56] Regimes $A_{1g}/A_{2g} > 0.60$, $A_{1g}/A_{2g} < 0.50$, and in between correspond to non-oxidized, oxidized, and partially oxidized states, respectively.[49,57] The position of the h-BN E_{2g} peak at 1368.4 cm^{-1} (Figure 3a) confirms that the h-BN used here has been successfully exfoliated into monolayers because this value is a typical literature value for monolayer, it is a shifted value compared to the bulk (1366.6 ± 0.2 cm^{-1}).[58,59] The h-BN Raman peak remained unchanged during the described experiments and will be excluded from further analysis.

The temporal evolution of the oxidation process was monitored by Raman spectroscopy. In the boxes, in Figure 3b–d the spectra obtained during the time-dependent measurements are presented. Figure 3b reveals a decreasing A_{1g}/A_{2g} ratio, indicating the oxidation of BP. The peak intensity ratio stabilized after 100 min, thus marking the end of the surface oxidation of the BP flakes. These spectra correspond to the reaction path in Figure 1a. The process was repeated on a pristine BP flake, but this time, exfoliated h-BN was drop-casted onto the partially oxidized BP after 50 min (path Figure 1b, spectral series Figure 3c) and the sample was allowed to stay at ambient conditions for 50 more minutes. The A_{1g} peak decreased only up to the point when h-BN was added. Afterward, the A_{1g}/A_{2g} ratio remained unchanged, indicating that the partially oxidized state of BP was preserved by the h-BN coating. Spectral series Figure 3d (corresponding to path Figure 1c) demonstrates that if monolayer h-BN is dropped over the pristine BP sample at $t = 0$ min, then peak intensity ratios will remain intact during the whole observation period, indicating a full oxidation protection effect by h-BN.

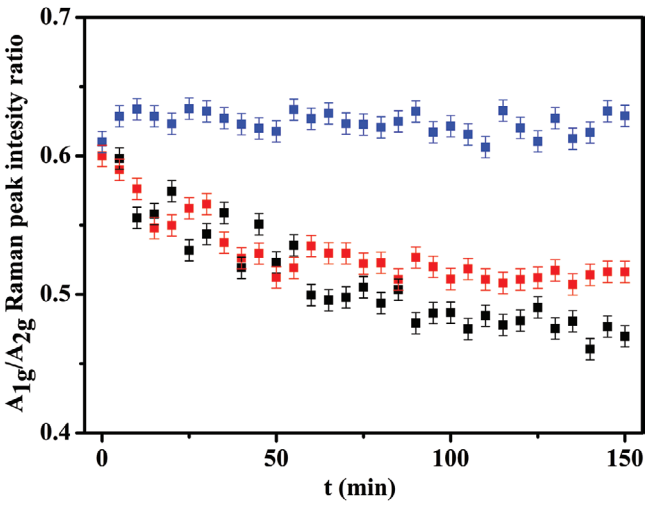

Figure 4. A_{1g}/A_{2g} Raman peak intensity ratios as a function of time during ambient BP oxidation (black dots), BP oxidation with the addition of h-BN mid-process (red dots), and BP fully protected from oxidation by h-BN (blue dots). Error bars represent the stochastic spatial variation of the intensity ratio as calculated from the latter dataset.

Figure 4 presents a quantitative analysis of the spectral series described in Figure 3b–d by drawing BP's Raman A_{1g}/A_{2g} ratio against time. Black dots indicate the oxidation behavior of untreated BP in ambient conditions (final A_{1g}/A_{2g} ratio <0.50), blue dots demonstrate the protective effect of monolayer h-BN deposition (A_{1g}/A_{2g} ratio >0.60 continuously), and red dots depict the time series when the protective coating was applied only after 50 min of spontaneous BP oxidation, effectively halting any further A_{1g}/A_{2g} ratio decrease at around $A_{1g}/A_{2g} = 0.53$ ratio.

X-ray photoelectron spectroscopy was utilized to characterize the fully protected BP + h-BN sample after the 150 min of ambient air exposure shown in Figure 4. High-resolution spectra for P 2p, B 1s, N 1s, O 1s, and Si 2p are presented in **Figure 5**.

The quantitative analysis of the XPS spectra revealed that the atomic ratio P to N is close to 1:1, therefore, we may assume that the BP: h-BN ratio in the fully protected sample was also 1:1. Most of the oxygen is allocated to the SiO_2 layer of the substrate, and a significant amount of carbonaceous species originating from the adsorbed acetone exfoliating agent were also found. 81.35% atomic% of the phosphorus was in the zero oxidation state and the remaining 18.65% could be identified as oxidized phosphorus. This enables us to estimate the h-BN coverage in the fully protected sample. Since oxygen can penetrate neither the h-BN surface nor the BP – h-BN edge gap (see below), we may assume that the phosphorus atoms transformed into P(ox) because they were not covered by h-BN flakes, while the remaining 81.35% phosphorus was kept intact at zero oxidation state because they were covered by h-BN. The actual amount of h-BN covered BP flake area could be larger than that because some of the oxidized P atoms can be present even at the edges of BP flakes apparently covered by h-BN from the top. Consequently, the actual coverage of BP flakes by h-BN in the fully protected sample is likely to be in the 81%–100% range.

Theoretical simulations were performed using the PM6-D3 method in order to understand the mechanism of this protective effect. In **Figure 6**a the partial charge distribution obtained from the Mulliken population analysis of the BP/h-BN system (before the interaction with the O_2 molecules) can be observed. As it can be seen, while the BP presents a well similar distributed charge, the h-BN sheet shows an alternation of negative (excess of electrons on N atoms) and positive (lack of electrons on B atoms) partial charges, which can influence how the O_2 molecules will attack/attach to the h-BN and/or BP layer. In Figure 6b we present the BP/h-BN/O_2 system after the geometry optimization. The O_2 molecules attack the uncovered BP parts, as well the h-BN edges, but they remain around 3.5 Å away from the h-BN surface. O_2 molecules cannot

© 2022 Wiley-VCH GmbH

21967350, 2022, 24, Downloaded from https://onlinelibrary.wiley.com/doi/10.1002/admi.202200857 by University Of Szeged, Wiley Online Library on [03/07/2023]. See the Terms and Conditions (https://onlinelibrary.wiley.com/terms-and-conditions) on Wiley Online Library for rules of use; OA articles are governed by the applicable Creative Commons License

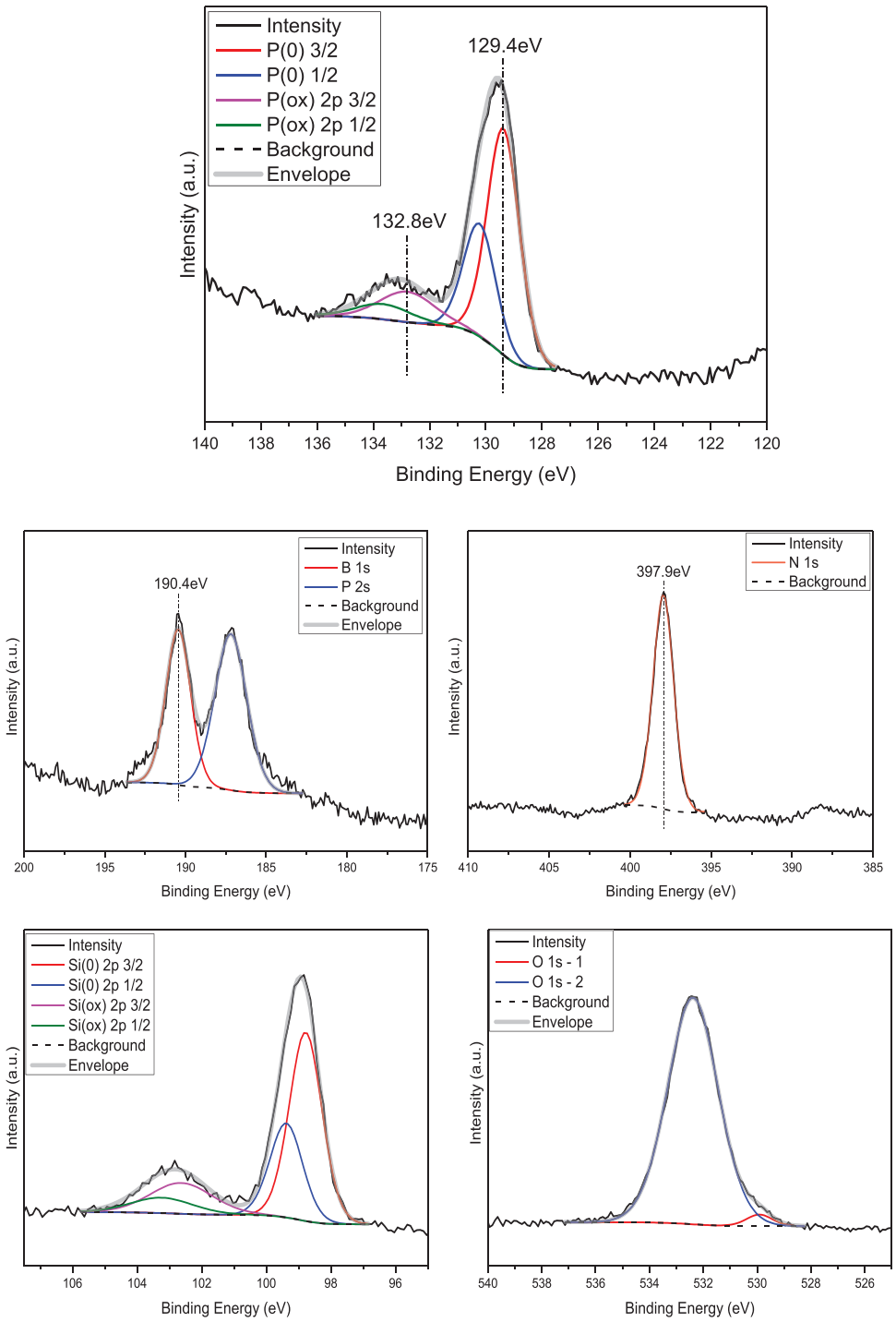

Figure 5. Characteristic XPS spectra of P, B, N, Si, and O collected on the same fully protected BP + h-BN sample after 150 min of ambient air exposure.

be spotted between the BP and h-BN, indicating that the part covered by h-BN sheets was protected from oxidation. We can understand this result based on the charge distribution on h-BN and the compound electronegativity. As the h-BN sheet presents negative and positive regions due to the difference in electronegativity between the B and N atoms when an O_2 molecule approaches the surface, it will face both attractive and repulsive forces, which cannot be energetically favorable for the O_2 molecule interaction. However, due to the constant charge distribution BP monolayer (see Figure 6a), there is no region in which strong repulsion or attraction would be present when an O_2 molecule approaches it. This fact, together with a lower electronegativity of the P atoms compared to O, indicates that if both flakes expose their oxygen-accessible surfaces, the oxidation of BP will be favored over the oxidation of h-BN. This result is in full agreement with the well-known oxidation

© 2022 Wiley-VCH GmbH

21967350, 2022, 24, Downloaded from https://onlinelibrary.wiley.com/doi/10.1002/admi.202200857 by University Of Szeged, Wiley Online Library on [03/07/2023]. See the Terms and Conditions (https://onlinelibrary.wiley.com/terms-and-conditions) on Wiley Online Library for rules of use; OA articles are governed by the applicable Creative Commons License

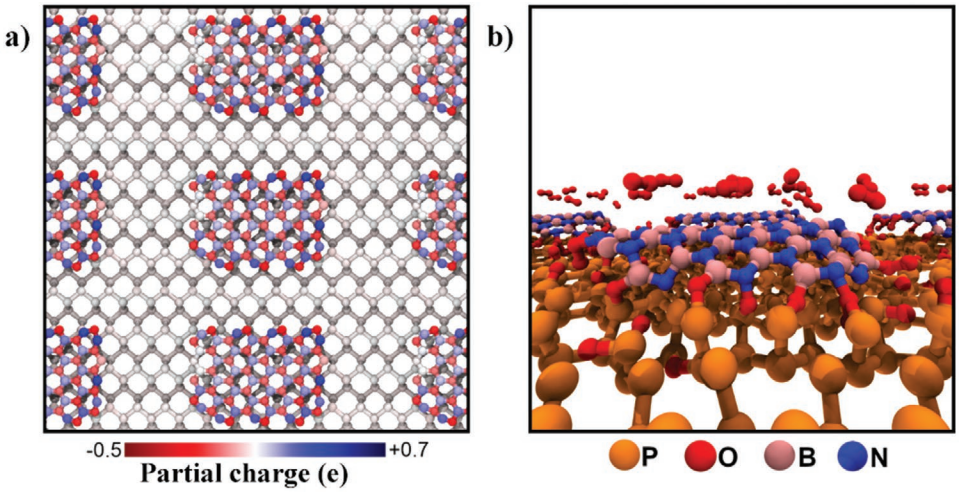

Figure 6. Optimized structure of a) BP/h-BN and b) BP/h-BN/O_2 systems. In (a), the atoms are colored to represent their partial charge according to the RWG scale presented at the bottom of the figure.

resistance of h-BN. Furthermore, we can notice in Figure 6b that the O_2 molecules interact with the h-BN edges due to the presence of N and B dangling bonds. This fact also favors the BP encapsulation, since the passage of other O_2 molecules through the BP and h-BN gap will be blocked. Therefore, our results suggest that the BP oxidation will be prevented by the h-BN mainly due to two factors: i) The h-BN charge distribution which prevents the O_2 molecules to interact with it, keeping them away from its surface, and ii) when the O_2 molecules attack the h-BN edges, it creates a barrier for the other O_2 molecules to diffuse freely inside the gap between the BP and h-BN layers.

3. Conclusion

We presented the first experimental evidence on employing Raman spectroscopy for real-time following the oxidation of phosphorene when depositing monolayer h-BN onto its surface that can fully prevent its ambient oxidation. Moreover, casting h-BN layers onto a partially oxidized BP sample can halt its oxidation, thus opening the path toward oxidation-induced bandgap modulation in air-stable real-life devices based on phosphorene. Monolayer BP and h-BN were obtained by sonication in acetone, samples were prepared by simple drop-casting on Si wafers, and observations about the oxidation state were made on the basis of BP's Raman A_{1g}/A_{2g} peak ratio. The experimental findings match theoretical simulation results very well and we have an indication of how the oxygen molecule approaches the heterostructure. The latter suggests that the oxidation of BP is prevented because of i) the charge distribution of h-BN, which keeps O_2 molecules from interacting with its surface, and ii) the fact that the first O_2 molecules in contact react with the edges of h-BN, thus creating a barrier for subsequently arriving O_2 molecules that cannot diffuse freely inside the BP and h-BN gap.

4. Experimental Section

Bulk h-BN was purchased from Sigma–Aldrich, bulk BP crystals were purchased from HQ+ Graphene (Groningen, The Netherlands). BP crystals were stored in the dark under an argon atmosphere. The exfoliation was done by measuring 4 mg of BP into a glass vial with 10 ml of acetone, the same amounts were used in the case of h-BN in a separate vial. The glass vials were closed with a septum cap and the samples were exfoliated using a sonication bath (120 W, 35 kHz) at 23 °C. The BP sample was sonicated for 20 h, whereas the sonication time for h-BN was 2 h. Then, the dispersions were centrifuged at 4000 rpm for 20 min. Small, exfoliated flakes of BP and h-BN, were collected from the supernatant.

Raman spectra were recorded with a Bruker Sentera II confocal Raman microscope using a laser source with 532 nm wavelength and laser power of 2.50 mW, spectral resolution 4 cm^{-1}, optical objective 50x, aperture 50 × 1000 µm, with 3 coadditions, 50 s each measurement. The measurements were conducted by dropping the dispersions on a Si wafer, covered with 300 nm thick SiO_2. The morphological characteristics as the number and shape of exfoliated layers were examined with an FEI Tecnai G2 20 X Twin instrument (FEI Corporate Headquarters, Hillsboro, OR, USA) TEM by drop-casting the samples on lacey carbon film-coated copper grids of 200 mesh grid density using 200 kV accelerating voltage.

The actual coating experiments commenced by drop-casting, two drops of the exfoliated BP sol onto a clean silicon wafer under ambient conditions. Unprotected BP samples were fully oxidized according to Raman spectroscopy in 100 min (Figure 1a). The oxidation process could be stopped by depositing three drops of the h-BN sol after 50 min of oxidation (Figure 1b) and it could also be fully prevented by depositing three drops of the h-BN dispersion directly after the casting of the BP sample (Figure 1c).

XPS was measured on a Specs XPS instrument equipped with an XR50 dual anode X-ray source and a Phoibos 150 hemispherical electron analyzer. The Al Kα X-ray source was operated with 150 W (14 kV) power. The survey spectrum was acquired with a pass energy of 40 and 1 eV step size. High-resolution spectra were acquired with a pass energy of 20 and 0.1 eV step size. High-resolution spectra were corrected with a Shirley background and were referenced to the aliphatic component of the C 1s peak at 284.8 eV. All peak components were fit with a Gauss-Lorentzian product function with a 30% Lorentzian contribution. Quantification is calculated from the corresponding peak areas corrected with the Scofield cross-section-based relative sensitivity factors.

© 2022 Wiley-VCH GmbH

21967350, 2022, 24, Downloaded from https://onlinelibrary.wiley.com/doi/10.1002/admi.202200857 by University Of Szeged, Wiley Online Library on [03/07/2023]. See the Terms and Conditions (https://onlinelibrary.wiley.com/terms-and-conditions) on Wiley Online Library for rules of use; OA articles are governed by the applicable Creative Commons License

To have more insights on the BP oxidation prevention from h-BN encapsulation, we have performed theoretical simulations using the Hartree-Fock-based Parametric Method 6 (PM6).[60] In our simulations, our theoretical model consists of a rectangular supercell of 26.86 × 19.96 Å, with a BP monolayer (128 P atoms) with an h-BN sheet of 16.40 × 11.20 Å (39 B and 39 N atoms, with two armchair and two zig-zag sides, nonpassivated) centralized on top of it. With this configuration, we end up with ≈66% (34%) of the BP covered (uncovered) by h-BN. We did the geometry optimization (an energy minimization) of this BP/h-BN system, and the BP h-BN interlayer distance was 3.36 Å. Then, with the geometry optimized BP/h-BN system, we placed randomly 32 O_2 molecules on top of it around 2.2 Å distant from BP and h-BN. We did another geometry optimization with this BP/h-BN/O_2 system to study BP oxidation. All simulations were performed with MOPAC2016.[61] For the geometry optimizations, a termination criterium for the gradient norm of 0.05 kcal mol^{-1} $Å^{-1}$ is employed and the D3 dispersion corrections for van der Waals interactions is applied.[62] Periodic boundary conditions were allowed for *x* and *y* directions.

Statistical Analysis: The collected Raman spectra were baseline corrected by subtracting a linear baseline fitted to two featureless sections of the spectrum located at lower and higher wavenumbers than the three monitored phosphorene peaks. The baseline-corrected spectra were normalized to the intensity of the A_{2g} peak of black phosphorus. Electron microscopic images were taken on three different spots of each sample that were separated by a distance of at least 1000 times the length of a typical black phosphorus flake. Images were considered characteristic of the whole sample if the morphological features observed on them could be easily identified at all three spots. The peak intensity ratios shown in Figure 4 were presented as actual measured values without any averaging. Error bars in Figure 4 were calculated by assuming that the variation in the peak intensity ratio of the fully protected BP flakes (blue dots in Figure 4) is due to stochastic effects originating from the unavoidable spatial inhomogeneity of drop-casted samples. The unbiased estimation of the standard deviation of the A_{1g}/A_{2g} peak intensity ratio was calculated from these $N = 31$ data points, and this estimation is depicted as error bar lengths for all datasets in Figure 4. Our previous, independent calibration experiments have demonstrated that the variation peak intensity ratio due to instrumental error and the uncertainty of the time measurement are both negligible compared to the spatial variation, therefore, these are not shown in the figure. Statistical tests were not performed. Microsoft Excel and OriginLab Origin were used in the data analysis.

Acknowledgements

Project no. TKP2021-NVA-19 has been implemented with the support, provided by the Ministry of Innovation and Technology of Hungary from, the National Research, Development, and Innovation Fund, financed under, the TKP2021-NVA funding scheme. Support from the Hungarian National Research, Development, and Innovation Office through project K138714 is acknowledged. EFO thanks the Brazilian agency FAPESP (Grants 2013/08293-7, 2016/18499-0, and 2019/07157-9) for financial support. Computational support from the Center for Computational Engineering and Sciences at Unicamp through the FAPESP/CEPID Grant No. 2013/08293-7 and the Center for Scientific Computing (NCC/GridUNESP) of São Paulo State University (UNESP) is also acknowledged.

Conflict of Interest

The authors declare no conflict of interest.

Data Availability Statement

The data that support the findings of this study are available from the corresponding author upon reasonable request.

Keywords

h-BN, 2D materials, Raman spectroscopy, passivation, oxidation, phosphorene

Received: April 18, 2022
Revised: May 23, 2022
Published online: July 20, 2022

[1] X. Zhang, A. Beyer, *Nanoscale* **2021**, *13*, 1443.
[2] X. Song, J. Hu, H. Zeng, *J. Mater. Chem. C* **2013**, *1*, 2952.
[3] Z. Guo, H. Zhang, S. Lu, Z. Wang, S. Tang, J. Shao, Z. Sun, H. Xie, H. Wang, X. F. Yu, P. K. Chu, *Adv. Funct. Mater.* **2015**, *25*, 6996.
[4] B. Li, C. Lai, G. Zeng, D. Huang, L. Qin, M. Zhang, M. Cheng, X. Liu, H. Yi, C. Zhou, F. Huang, S. Liu, Y. Fu, *Small* **2019**, *15*, 180456.
[5] R. Boddula, A. M. Asiri, *Black Phosphorus*, Springer International Publishing, Cham **2020**.
[6] B. Bienvenu, H. Amara, F. Ducastelle, L. Sponza, *Phys. Rev. B* **2020**, *102*, 035415.
[7] Y. Liu, M. Chen, S. Yang, *InfoMat* **2021**, *3*, 231.
[8] J. F. Gómez-Pérez, J. D. Correa, C. B. Pravda, Z. Kónya, Á. Kukovecz, *J. Phys. Chem. C* **2020**, *124*, 24066.
[9] H.-S. Ra, A.-Y. Lee, D.-H. Kwak, M.-H. Jeong, J.-S. Lee, *ACS Appl. Mater. Interfaces* **2018**, *10*, 925.
[10] D. Yu, J. Li, T. Wang, X. She, Y. Sun, J. Li, L. Zhang, X.-F. Yu, D. Yang, *Phys. Status Solidi – Rapid Res. Lett.* **2020**, *14*, 1900697.
[11] G. Korotcenkov, *Sensors (Switzerland)* **2019**, *19*, 1010.
[12] Q. Li, J. T. Wu, Y. Liu, X. M. Qi, H. G. Jin, C. Yang, J. Liu, G. L. Li, Q. G. He, *Anal. Chim. Acta* **2021**, *1170*, 338480.
[13] M. Donarelli, L. Ottaviano, L. Giancaterini, G. Fioravanti, F. Perrozzi, C. Cantalini, *2D Mater.* **2016**, *3*, 025002.
[14] Y. Zhang, Q. Jiang, P. Lang, N. Yuan, J. Tang, *J. Alloys Compd.* **2021**, *850*, 156580.
[15] I. Fasolino, A. Soriente, M. Caporali, M. Serrano-Ruiz, M. Peruzzini, L. Ambrosio, M. G. Raucci, *Sci. Rep.* **2021**, *11*, 5856.
[16] S. Nangare, P. Patil, *Crit. Rev. Anal. Chem.* **2021**, https://doi.org/10.1080/10408347.2021.1927669.
[17] H. Mu, W. Yu, J. Yuan, S. Lin, G. Zhang, *Mater. Futur.* **2022**, *1*, 012301.
[18] A. Pandey, A. N. Nikam, G. Fernandes, S. Kulkarni, B. S. Padya, R. Prassl, S. Das, A. Joseph, P. K. Deshmukh, P. O. Patil, S. Mutalik, *Nanomaterials* **2021**, *11*, 13.
[19] N. Clark, L. Nguyen, M. J. Hamer, F. Schedin, E. A. Lewis, E. Prestat, A. Garner, Y. Cao, M. Zhu, R. Kashtiban, J. Sloan, D. Kepaptsoglou, R. V. Gorbachev, S. J. Haigh, *Nano Lett.* **2018**, *18*, 5373.
[20] Y. Liu, P. Gao, T. Zhang, X. Zhu, M. Zhang, M. Chen, P. Du, G. W. Wang, H. Ji, J. Yang, S. Yang, *Angew. Chem., Int. Ed.* **2019**, *58*, 1479.
[21] R. Guo, Y. Zheng, Z. Ma, X. Lian, H. Sun, C. Han, H. Ding, Q. Xu, X. Yu, J. Zhu, W. Chen, *Appl. Surf. Sci.* **2019**, *496*, 143688.
[22] S. Wu, K. S. Hui, K. N. Hui, *Adv. Sci.* **2018**, *5*, 1700491.
[23] Z. Shi, X. Ren, H. Qiao, R. Cao, Y. Zhang, X. Qi, H. Zhang, *J. Photochem. Photobiol., C* **2020**, *43*, 100354.
[24] R. A. Doganov, E. C. T. O'Farrell, S. P. Koenig, Y. Yeo, A. Ziletti, A. Carvalho, D. K. Campbell, D. F. Coker, K. Watanabe, T. Taniguchi, A. H. C. Neto, B. Özyilmaz, *Nat. Commun.* **2015**, *6*, 6647.
[25] G. C. Constantinescu, N. D. M. Hine, *Nano Lett.* **2016**, *16*, 2586.
[26] J. Gómez-Pérez, B. Barna, I. Y. Tóth, Z. Kónya, Á. Kukovecz, *ACS Omega* **2018**, *3*, 12482.
[27] S. Thurakkal, D. Feldstein, R. Perea-Causín, E. Malic, X. Zhang, *Adv. Mater.* **2021**, *33*.

© 2022 Wiley-VCH GmbH

21967350, 2022, 24, Downloaded from https://onlinelibrary.wiley.com/doi/10.1002/admi.202200857 by University Of Szeged, Wiley Online Library on [03/07/2023]. See the Terms and Conditions (https://onlinelibrary.wiley.com/terms-and-conditions) on Wiley Online Library for rules of use; OA articles are governed by the applicable Creative Commons License

[28] I. V. Sankar, J. Jeon, S. K. Jang, J. H. Cho, E. Hwang, S. Lee, *Heterog. Integr. 2D Mater.: Recent Adv. Fabr. Funct. Device Appl.* **2019**, *14*, 1930009.
[29] Y. Liu, N. O. Weiss, X. Duan, H. C. Cheng, Y. Huang, X. Duan, *Nat. Rev. Mater.* **2016**, *1*, 16042.
[30] A. K. Geim, I. V. Grigorieva, *Nature* **2013**, *499*, 419.
[31] J. M. J. Lopes, *Prog. Cryst. Growth Charact. Mater.* **2021**, *67*, 100522.
[32] D. Golberg, Y. Bando, Y. Huang, T. Terao, M. Mitome, C. Tang, C. Zhi, *ACS Nano* **2010**, *4*, 2979.
[33] A. Pakdel, C. Zhi, Y. Bando, D. Golberg, *Mater. Today* **2012**, *15*, 256.
[34] Y. Lin, J. W. Connell, *Nanoscale* **2012**, *4*, 6908.
[35] A. El Sachat, F. Alzina, C. M. Sotomayor Torres, E. Chavez-Angel, *Nanomaterials* **2021**, *11*, 175.
[36] H. Song, H. Wu, T. Ren, S. Yan, T. Chen, Y. Shi, *Nano Res.* **2021**, *14*, 4386.
[37] Q. Li, M. Liu, Y. Zhang, Z. Liu, *Small* **2016**, *12*, 32.
[38] L. Shen, Y. Zhao, Y. Wang, R. Song, Q. Yao, S. Chen, Y. Chai, *J. Mater. Chem. A* **2016**, *4*, 5044.
[39] J. Wang, F. Ma, M. Sun, *RSC Adv.* **2017**, *7*, 16801.
[40] Y. Cai, G. Zhang, Y. W. Zhang, *J. Phys. Chem. C* **2015**, *119*, 13929.
[41] A. Avsar, I. J. Vera-Marun, J. Y. Tan, K. Watanabe, T. Taniguchi, A. H. Castro Neto, B. Özyilmaz, *ACS Nano* **2015**, *9*, 4138.
[42] Y. Cao, A. Mishchenko, G. L. Yu, E. Khestanova, A. P. Rooney, E. Prestat, A. V. Kretinin, P. Blake, M. B. Shalom, C. Woods, J. Chapman, G. Balakrishnan, I. V. Grigorieva, K. S. Novoselov, B. A. Piot, M. Potemski, K. Watanabe, T. Taniguchi, S. J. Haigh, A. K. Geim, R. V. Gorbachev, *Nano Lett.* **2015**, *15*, 4914.
[43] S. Sinha, Y. Takabayashi, H. Shinohara, R. Kitaura, *2D Mater.* **2016**, *3*, 035010.
[44] M. Birowska, J. Urban, M. Baranowski, D. K. Maude, P. Plochocka, N. G. Szwacki, *Nanotechnology* **2019**, *30*, 195201.
[45] C. Wang, J. Sun, B. Zhang, J. Zhang, X. Tao, *Appl. Surf. Sci.* **2017**, *423*, 1003.
[46] E. Gao, S. Z. Lin, Z. Qin, M. J. Buehler, X. Q. Feng, Z. Xu, *J. Mech. Phys. Solids* **2018**, *115*, 248.
[47] C. R. Ryder, J. D. Wood, S. A. Wells, Y. Yang, D. Jariwala, T. J. Marks, G. C. Schatz, M. C. Hersam, *Nat. Chem.* **2016**, *8*, 597.
[48] S. Wild, V. Lloret, N. Scheuschner, R. Gillen, U. Mundloch, J. Maultzsch, M. Varela, F. Hauke, A. Hirsch, *J. Am. Chem. Soc.* **2017**, *139*, 10432.
[49] A. Favron, E. Gaufrès, F. Fossard, A. P. Heureux, N. Y. Tang, P. L. Lévesque, A. Loiseau, R. Leonelli, S. Francoeur, R. Martel, *Nat. Mater* **2015**, *14*, 826.
[50] J. M. Urban, M. Baranowski, A. Surrente, D. Wlodarczyk, A. Suchocki, G. Long, Y. Wang, L. Klopotowski, N. Wang, D. K. Maude, P. Plochocka, *Nanoscale* **2017**, *9*, 19298.
[51] Z. X. Hu, X. Kong, J. Qiao, B. Normand, W. Ji, *Nanoscale* **2016**, *8*, 2740.
[52] B. Zou, Y. Wei, Y. Zhou, D. Ke, X. Zhang, M. Zhang, C. T. Yip, X. Chen, W. Li, H. Sun, *Nanoscale Horiz.* **2021**, *6*, 809.
[53] S. Liang, M. N. Hasan, J. H. Seo, *Nanomaterials* **2019**, *9*, 566.
[54] G. Abellµn, V. Lloret, U. Mundloch, M. Marcia, C. Neiss, A. Gçrling, M. Varela, F. Hauke, A. Hirsch, *Noncovalent Functionalization of Black Phosphorus* **2016**, *128*, 14777.
[55] Y. L. Hsieh, W. H. Su, C. C. Huang, C. Y. Su, *ACS Appl. Mater. Interfaces* **2020**, *12*, 37375.
[56] D. Hanlon, C. Backes, E. Doherty, C. S. Cucinotta, N. C. Berner, C. Boland, K. Lee, A. Harvey, P. Lynch, Z. Gholamvand, S. Zhang, K. Wang, G. Moynihan, A. Pokle, Q. M. Ramasse, N. McEvoy, W. J. Blau, J. Wang, G. Abellan, F. Hauke, A. Hirsch, S. Sanvito, D. D. O'Regan, G. S. Duesberg, V. Nicolosi, J. N. Coleman, *Nat. Commun.* **2015**, *6*, 8563.
[57] J. Gómez-Pérez, B. Barna, I. Y. Tóth, Z. Kónya, Á. Kukovecz, *ACS Omega* **2018**, *3*, 12482.
[58] R. V. Gorbachev, I. Riaz, R. R. Nair, R. Jalil, L. Britnell, B. D. Belle, E. W. Hill, K. S. Novoselov, K. Watanabe, T. Taniguchi, A. K. Geim, P. Blake, *Small* **2011**, *7*, 465.
[59] Q. Cai, D. Scullion, A. Falin, K. Watanabe, T. Taniguchi, Y. Chen, E. J. G. Santos, L. H. Li, *Nanoscale* **2017**, *9*, 3059.
[60] J. J. P. Stewart, *J. Mol. Model.* **2007**, *13*, 1173.
[61] MOPAC2016, James J. P. Stewart, *Stewart Computational Chemistry*, Colorado Springs, CO, USA **2016**.
[62] S. Grimme, J. Antony, S. Ehrlich, H. Krieg, *J. Chem. Phys.* **2010**, *132*, 154104.

© 2022 Wiley-VCH GmbH

21967350, 2022, 24, Downloaded from https://onlinelibrary.wiley.com/doi/10.1002/admi.202200857 by University Of Szeged, Wiley Online Library on [03/07/2023]. See the Terms and Conditions (https://onlinelibrary.wiley.com/terms-and-conditions) on Wiley Online Library for rules of use; OA articles are governed by the applicable Creative Commons License